

A fluorescence activatable reporter of flavivirus NS2B-NS3 protease activity enables live imaging of infection in single cells and viral plaques

Jorge L. Arias-Arias¹, Derek J. MacPherson², Maureen E. Hill², Jeanne A. Hardy², and Rodrigo Mora-Rodríguez^{1*}

From ¹Centro de Investigación en Enfermedades Tropicales (CIET), Facultad de Microbiología, Universidad de Costa Rica, San José 11501-2060, Costa Rica; ²Department of Chemistry, 104 LGRT, 710 N. Pleasant St., University of Massachusetts Amherst, MA 01003, USA

Running title: *A cell-based fluorescent reporter for flavivirus infection*

*corresponding author: Rodrigo Mora-Rodríguez: Centro de Investigación en Enfermedades Tropicales, Facultad de Microbiología, Universidad de Costa Rica, Ciudad Universitaria Rodrigo Facio, San Pedro de Montes de Oca, San José 11501-2060, Costa Rica; phone (506) 2511-8635; rodrigo.morarodriguez@ucr.ac.cr

Keywords: cell death, dengue virus (DENV), flavivirus, fluorescence, internal cleavage, NS2B-NS3, protease, plaque assay, cell-based reporter, Zika virus (ZIKV)

ABSTRACT

The genus *Flavivirus* in the family *Flaviviridae* comprises many medically important viruses, such as dengue virus (DENV), Zika virus (ZIKV), and yellow fever virus (YFV). The quest for therapeutic targets to combat flavivirus infections requires a better understanding of the kinetics of virus–host interactions during infections with native viral strains. However, this is precluded by limitations of current cell-based systems for monitoring flavivirus infection in living cells. In the present study, we report the construction of fluorescence activatable sensors to detect the activities of flavivirus NS2B-NS3 serine proteases in living cells. The system consists of GFP-based reporters that become fluorescent upon cleavage by recombinant DENV-2/ZIKV proteases *in vitro*. A version of this sensor containing the flavivirus internal NS3 cleavage site linker reported the highest fluorescence activation in stably transduced mammalian cells upon DENV-2/ZIKV infection. Moreover, the onset of fluorescence correlated with viral protease activity. A far-red version of this flavivirus sensor had the best signal-to-noise ratio in a fluorescent Dulbecco's plaque assay, leading to the construction of a multi-reporter platform combining the flavivirus sensor with reporter dyes for detection of chromatin condensation and cell death, enabling studies of viral plaque formation with single-cell resolution. Finally, the application of this platform enabled the study of cell-population

kinetics of infection and cell death by DENV-2, ZIKV, and YFV. We anticipate that future studies of viral infection kinetics with this reporter system will enable basic investigations of virus–host interactions and facilitate future applications in antiviral drug research to manage flavivirus infections.

The genus *Flavivirus* in the family *Flaviviridae* comprises more than 70 species of arthropod-borne viruses (arboviruses) that are transmitted to vertebrates by infected mosquitoes or ticks, producing diseases in animals and humans, including many medically important viruses like West Nile virus (WNV), yellow fever virus (YFV), St. Louis encephalitis virus (SLEV), dengue virus (DENV), Japanese encephalitis virus (JEV), Zika virus (ZIKV), and Tick-borne encephalitis virus (TBEV) (1).

The genome of flaviviruses is a positive sense RNA of ~11 kb that encodes three structural proteins, i.e. capsid (C), membrane precursor (prM), and envelope (E), and seven nonstructural proteins, i.e. NS1, NS2A, NS2B, NS3, NS4A, NS4B, and NS5. These proteins initially form a precursor polyprotein (NH₂-C-prM-E-NS1-NS2A-NS2B-NS3-NS4A-NS4B-NS5-COOH) that is cleaved by both cellular and viral proteases to release the mature viral proteins (2). The flavivirus serine protease NS2B-NS3 consists of the N-

terminal domain of the NS3 protein, associated with the membrane-resident NS2B cofactor to form an active complex. This viral protease cleaves the precursor polyprotein at the NS2A/NS2B, NS2B/NS3, NS3/NS4A, and NS4B/NS5 junctions, as well as at internal sites within C, NS2A, NS3, and NS4A (3–5).

Flaviviruses have continued to emerge in recent years and together represent a global threat responsible for pandemics associated with encephalitis and hemorrhagic fever diseases for which there are no specific treatments available other than supportive care upon hospitalization (2). Moreover, the development of successful human vaccines seems to be challenging for some flaviviruses. Although YFV, JEV, and TBEV vaccines are highly effective, the development of vaccines for other flaviviruses like WNV and DENV have presented some drawbacks and safety concerns (6–8). This situation partially arises from the limitations of clinical studies and although there are established animal models for flaviviruses, they do not faithfully reproduce all the clinical manifestations observed in the human host (9, 10). Therefore, post-mortem studies and cell culture models still being an important approach to study flavivirus diseases (11–13), especially for the quest of novel therapeutic targets to combat these infections, either on the virus or on the host (14, 15).

Currently, the identification of flavivirus-infected cells relies on either immunostaining of viral proteins (12) the application of recombinant reporter replicons or viral genomes (16–20), or the use of cell-based molecular reporters of the NS2B-NS3 activity (21–23). Antibody staining techniques require both fixation and permeabilization due to the lack of flavivirus expressed proteins directly on the cell surface of infected cells as a part of the viral replication cycle (2, 24, 25) which precludes their application for live-cell imaging. Reporter replicons and viral genomes allow kinetic studies in living cells, but are limited to molecular clones and thus, not suitable to study clinical isolates or native virus strains. In this respect, genetically-encoded molecular reporters monitoring the flavivirus NS2B-NS3 proteolytic activity upon infection are an advantageous approach that is suitable for live-cell imaging studies of native flavivirus strains.

Previously, we developed a series of caspase-activatable reporters by fusing, via a linker containing the caspase-3/-7 cleavage site DEVD, a hydrophobic quenching peptide to the C-terminus of a fluorescent protein (26–28). This quenching peptide inhibits the maturation of the chromophore in the fluorescent protein until it is proteolytically removed by an active caspase, fully restoring the fluorescence (26, 27). In the present study, we developed genetically-encoded flavivirus molecular reporters by inserting a flaviviral NS2B-NS3 cleavage site into our caspase-activatable GFP (CA-GFP) (26) or caspase-activatable mNeptune (CA-mNeptune) (28), giving rise to the flavivirus-activatable GFP (FlaviA-GFP) and flavivirus-activatable mNeptune (FlaviA-mNeptune) reporters, respectively. To our knowledge, this is the first fluorescence activatable molecular reporter system for live-cell imaging of the infection by both reference and native strains of flaviviruses like DENV, ZIKV, and YFV.

Results

Fluorescence activatable GFP-based reporters of flavivirus NS2B-NS3 protease activity become fluorescent upon cleavage by recombinant DENV-2/ZIKV proteases in vitro

We based the design of a molecular sensor for flavivirus proteases on our previously reported CA-GFP sensor that comprises GFP, a linker for caspase cleavage and a C-terminal quenching peptide (26–28). However, we encountered several limitations for the development of the new sensor, mainly with the linker sequence for the reporter function. This led us to envisage several alternative designs by changing the linker sequence. Indeed, we generated several variants of the reporter that remained uncleaved and/or non-fluorescent upon DENV-2 NS2B-NS3 protease treatment *in vitro* (Table S1). Therefore, we designed a linker based on previously characterized flavivirus polyprotein cleavage sites (29). After careful analysis and avoiding the formation of cleavage sites for other cellular proteases within the resulting protein sequence of the sensor (http://web.expasy.org/peptide_cutter/), we selected the cleavage sequences that define the linker. Three variants of this reporter were constructed by changing the linker sequence: ZIKVA-GFP (ZIKV polyprotein NS2B/NS3

cleavage site linker), DENV2A-GFP (DENV-2 polyprotein NS2B/NS3 cleavage site linker), and FlaviA-GFP with the internal NS3 cleavage site present in many members of the *Flavivirus* genus (3, 5, 30). Using these variants of the reporter, we verified the cleavage *in vitro* by Coomassie blue-stained SDS-PAGE gels (Fig. 1A, 1B, and S1) and the fluorescence activation (Fig. 1C) to evaluate at the protein level the potential of these linkers to be used within reporters of viral protease activity.

Purified recombinant DENV-2 NS2B-NS3 protease (Fig. 1A, left panel) or ZIKV NS2B-NS3 protease (Fig. 1A, right panel) were added to the three purified flavivirus activatable-GFP reporter proteins. The DENV-2 NS2B-NS3 protease band was observed at 25 kDa and the ZIKV NS2B-NS3 protease was located below 20 kDa, whereas all three full-length reporter proteins appeared above 30 kDa. To determine the location of the cleaved reporters, we generated a truncated variant of the FlaviA-GFP reporter protein (tRep/control) by inserting a stop codon downstream of the cleavage site in the DNA sequence of the linker. The bands of the cleaved reporters appeared between the 25 kDa and the 30 kDa markers. The cleavage kinetics of the reporters can be observed over time for the three variants tested (Fig. 1A and 1B).

The intensities of these bands were quantified and a ratio of the cleaved reporter to the total amount of reporter protein for each time point was calculated. The results are displayed as time-resolved cleavage efficiency (%) to compare among the different variants of the reporter (Fig. 1B). The DENV-2 NS2B-NS3 protease has very similar cleavage kinetics for the three variants with some slight differences. Although the FlaviA-GFP reporter showed an earlier increase, the ZIKVA-GFP reporter also reached around 80% of cleavage efficiency. The DENV2A-GFP reached only approximately 50% efficiency (Fig. 1B, left panel). On the other hand, striking differences are observed for the cleavage efficiency of the three variants of the reporter by the ZIKV NS2B-NS3 protease. The ZIKVA-GFP reporter had a much earlier increase reaching almost 100% cleavage by 10 hours. In contrast, the FlaviA-GFP and the DENV2A-GFP variants reached only 40% of cleavage efficiency after 20 hours (Fig. 1B, right panel). These results indicate that the reporters are sensitive to flavivirus

protease cleavage as designed, although with different efficiencies and kinetics.

In order to determine whether these cleavage kinetics correlate with fluorescence activation of the reporters, we monitored the fluorescence signal of each reporter as a function of time and normalized it to the background signal for each construct, obtaining thereby a time-resolved signal-to-noise ratio for the fluorescence of the reporters. All three reporters showed an increased in this signal-to-noise ratio for both protease treatments, indicating that the cleavage of the constructs correlates with the fluorescence increase of the GFP. The ZIKVA-GFP reporter showed the highest increase in fluorescence for both protease treatments, followed by the FlaviA-GFP and the DENV2A-GFP. These results indicate that the increase of the signal-to-noise ratio is a sensitive marker of cleavage, especially for the ZIKVA-GFP reporter (Fig. 1C).

The FlaviA-GFP sensor reports the highest fluorescence increase in stably-transduced mammalian cells upon DENV-2/ZIKV infection

In order to validate our candidate GFP-based reporters of flavivirus NS2B-NS3 proteases, we generated three BHK-21 stable cell lines expressing each reporter. Upon DENV-2 or ZIKV infection at a low multiplicity of infection (MOI) of 0.25, we monitored the cellular fluorescence as a function of time using live imaging. A qualitative assessment of the images suggested that the cell fluorescence started to increase significantly at 48 hours post-infection (Fig. 2A and S2A). To quantify this increase, we constructed an image analysis pipeline using CellProfiler 2.0 to identify single cells based on their nuclei, recognize their cytoplasm (white outlines), classify them as live (blue dots) or dead cells (red outlines and dots) and quantify the total cell fluorescence (Fig. 2A and 2B). Our results showed that the viral-induced cytotoxicity started around 50-60 hours post-infection with DENV-2 and around 40-50 hours post-ZIKV infection (red dots, Fig. 2B). However, the cellular fluorescence started to increase in living cells (blue dots, Fig. 2B) approximately at 48 hours post-infection and we could quantify living cells with increased fluorescence until the end of this time course (96 hours). The population mean values for each condition are represented by the green continuous

lines. In order to compare the different variants of the reporter, we monitored the cell population kinetics of the flavivirus-activatable GFP sensor's fluorescence across multiple experiments and confirmed that the flavivirus internal NS3 cleavage site linker (AAQRRGRIG) confers the highest signal-to-noise ratio for reporting the infection of DENV-2 and ZIKV in stably-transduced BHK-21 cells (Fig. 2C). These results confirm that our GFP-based fluorescence activatable reporters of NS2B-NS3 protease activity can be used in living cells and that our variant harboring the flavivirus-conserved linker has the highest sensitivity to report viral infection for both DENV-2 and ZIKV at the single-cell level.

The fluorescence activation of the FlaviA-GFP reporter correlates with viral NS3 protease synthesis and activity in the cellular context

In order to validate the ability of the FlaviA-GFP construct to report the NS3 protease content in the cellular context, we first monitored the correlation of the reporter fluorescence with an anti-NS3 immunofluorescence staining. BHK-21 stable cells expressing the FlaviA-GFP reporter were infected with DENV-2 13538 and the NS3 protease was revealed by an immunofluorescence assay (IFA) with an anti-DENV NS3 protein antibody at 72 hours post-inoculation. High magnification images were obtained to study the cellular patterns of both fluorescent signals. The images showed a significant amount of colocalized fluorescence suggesting a correlation between cellular NS3 amounts and the fluorescent form of the FlaviA-GFP reporter (Fig. 3A). In order to confirm this correlation, we obtained low magnification images and quantified the total cellular intensity for both fluorescent signals in many single cells using CellProfiler 2.0. This quantification confirmed an important correlation (Fig. 3B), suggesting that the fluorescence of the FlaviA-GFP reporter arises due to the viral-induced synthesis of NS3 protease in the cells. To confirm this hypothesis, we monitored for 72 hours the cleavage kinetics of the FlaviA-GFP reporter in BHK-21 stable cells upon DENV-2 infection in parallel to the viral NS3 protease expression by western blot. Only the cells incubated with infectious DENV-2 showed a band of uncleaved NS3 protease. This signal was dim at 24 hours but became more evident at 48 and 72 hours, while a

band corresponding to the cleaved NS3 protease became visible at 48 hours post-infection, due to the autoproteolytic activity of NS3. On the other hand, the band of uncleaved FlaviA-GFP reporter was visible in lysates of cells incubated with UV-inactivated DENV-2, at all the times tested (Fig. 3C). In the presence of the infectious DENV-2 a slight band of cleaved FlaviA-GFP reporter appeared by 48 hours, correlating with the onset of autoproteolytic activity of the viral NS3. This band showed a strong increase after 72 hours post-infection similar to the increase of cleaved NS3 protease (Fig. 3C). This correlation was expected as both the FlaviA-GFP reporter and the viral NS3 protease contain the same flavivirus internal NS3 cleavage site (AAQRRGRIG). The cleavage of the NS3 protease itself therefore represents an excellent internal control for the NS3 protease activity in this experiment. Together, these results demonstrate that the fluorescence increase of the FlaviA-GFP reporter correlates with its proteolytic cleavage in the cellular context and this cleavage depends on the presence of active viral NS3 protease.

The FlaviA-mNeptune, a far-red version of the flavivirus sensor, reports the best signal-to-noise ratio in a DENV-2/ZIKV fluorescent plaque assay

To ascertain the ability of the FlaviA-GFP version of the sensor to report the cell population-based kinetics of infection, we designed an experimental protocol for a Dulbecco's plaque assay in 96-well plates. Briefly, confluent cell monolayers of BHK-21 cells stably expressing the FlaviA-GFP reporter were infected with decimal dilutions of a DENV-2 or ZIKV viral seed and incubated with a medium containing carboxymethylcellulose for 120 hours. The plaque-containing wells were completely imaged at 40X magnification and the whole-well images of cell monolayers were generated with the stitching function of the Gen5 3.0 software (BioTek). However, as shown in Figure 4B, the raw images of the FlaviA-GFP stable cell monolayers presented high backgrounds at low magnification in the green fluorescence channel, probably due to the autofluorescence of the phenol-red and the fetal bovine serum of the culture medium. An alternative medium without phenol-red (Gibco, 11935-046) was tested but showed an increase in cytotoxicity (data not shown). These images could be enhanced by increasing the contrast but thereby lost a

significant fraction of the cellular signal from the fluorescent viral plaques, as shown by the size comparison of the reporter plaques in the enhanced image to the plaques stained with an anti-NS3 antibody at 120 hours post-infection (Fig. 4B). Therefore, we envisaged a far-red version of our flavivirus reporter (FlaviA-mNeptune, Fig. 4A) based on our previously published CA-mNeptune sensor (28). We generated a new stable cell line with the far-red FlaviA-mNeptune reporter in order to compare the signal-to-noise ratio between the red fluorescent plaques and the green fluorescent plaques generated in FlaviA-GFP stable cells.

A time-based comparison of the plaque formation kinetics for both DENV-2 and ZIKV indicated that the FlaviA-mNeptune version of the reporter has a higher signal-to-noise ratio revealing earlier evidence of red fluorescent plaques 48-72 hours post-infection compared to the plaques produced by the fluorescence increase of the FlaviA-GFP reporter, which required 96-120 hours to become evident (Fig. 4C). To confirm the higher potential of the FlaviA-mNeptune reporter to reveal fluorescent viral plaques, we compared the size of the plaques for both types of reporters with the respective size of the same plaques stained with both an anti-NS3 antibody and crystal violet staining. We also identified the plaque outlines for both reporters using an image analysis protocol constructed in CellProfiler 2.0 based on cell-by-cell neighbor counts and image thresholding (Fig. 5A). The protocol identified much larger plaques for FlaviA-mNeptune infected cells compared to those of infected FlaviA-GFP cells. In addition, the size of the plaques generated in the FlaviA-mNeptune infected cells was very similar to the size of the plaques revealed by the NS3 labeling and the crystal violet staining (Fig. 4D).

Together, these results demonstrate that the mNeptune version of the flavivirus sensor reports the best signal-to-noise ratio in a Dulbecco's plaque assay, indicating that this reporter is a good marker of viral replication to study cell population-based kinetics of infection by this standard virological technique.

A multi-reporter platform to study viral plaques formation at a single-cell resolution reveals differences in cell-population kinetics of infection and cell death induction by several flaviviruses

To further investigate the potential application of our FlaviA-mNeptune reporter system to study the cell population-based kinetics of viral infection and plaque formation, we designed an experimental protocol combining three types of reporters. The FlaviA-mNeptune reporter was used as a surrogate marker of viral replication, Hoechst 33342 to stain chromatin condensation as an early marker of an ongoing apoptosis and SYTOX green to label nuclei of cells with permeabilized membranes as a late marker of cell death (Fig. 5A). We constructed an image analysis protocol in CellProfiler 2.0 to identify and characterize each individual plaque at a single-cell level. Briefly, the pipeline adds the images of the three channels into one (ImageMath) in order to identify all single cells with all possible combinations of the reporters (Cell identification). These cells are characterized by the quantification of their neighbors within a specified distance (Neighbor count) and filtered based on a minimal number of neighbors per cell (Filtered cells) to identify the plaque-forming cells. Then, a series of image enhancing steps enable us to perform the identification of plaques as new primary objects (Plaque identification). Finally, with the identified plaques we were able to relate the single cells to their corresponding plaques and quantify thereby the number of live-infected cells (red), live-infected cells with chromatin condensation (blue), and dead cells (green) (Fig. 5A). Moreover, the time-based monitoring of these parameters for each fluorescent viral plaque enabled us to study the cell-population kinetics of infection for ZIKV plaque formation until 120 hours (Fig. 5B). The quantification of these parameters indicated that the ratios of these three cell subpopulations over time are very similar among different plaques for this specific ZIKV strain, as depicted by the relatively low standard deviations observed (Fig. 5C). These results suggest that with the combination of a FlaviA-mNeptune reporter as a marker of infection with a reporter of chromatin condensation and a reporter for cell death, we can obtain a multi-reporter platform to characterize the infection kinetics induced by a specific viral strain.

In order to confirm the potential of this multi-reporter platform to reveal virus-specific differences in terms of viral replication, chromatin condensation, and cell death, we compared the fluorescent viral plaques generated upon the infection with different flaviviruses including DENV-2, ZIKV, and YFV. YFV represents an additional model to further validate the spectrum of application of our flavivirus reporter (Fig. S2B and S3) and to explore the heterogeneity in replication kinetics and cell death induction across multiple flaviviruses using our multi-reporter platform. The acquired images at 120 hours post-infection with DENV-2, ZIKV, and YFV show qualitative differences (Fig. 6A) that were examined using the image analysis protocol presented above (Fig. 5A). The artificial images generated by the image analysis protocol highlighted those differences (Single-cell plaque analysis, Fig. 6A). The identified plaques contained several subpopulations of infected cells: a central core of dead cells (green), surrounded by a ring of cells presenting chromatin condensation (blue) and another ring of live-infected cells (red). Nevertheless, the proportions of these cell subpopulations were very different for DENV-2, ZIKV, and YFV. Finally, the quantification of the percentage of cells corresponding to each subpopulation within each plaque confirmed the qualitative observations, indicating differential proportions of infection and induced cell death among the three viral species tested (Fig. 6B).

Next, we asked if the presence of either type of reporters (FlaviA-GFP and FlaviA-mNeptune) and dyes (Hoechst 33342 and SYTOX green) could affect the viral replication by comparing the plaque-forming units determined with the standard crystal violet staining on wild-type cells with those generated on both reporter cell lines at 96 hours post-infection with DENV-2, ZIKV, and YFV. A representative experiment for DENV-2 is shown in Figure S4A and the plaque count confirmed that there is no difference in viral replication among all three cell lines infected with all three viral species tested (Fig. S4B). This result validates that the behaviors observed for DENV-2, ZIKV, and YFV arise from intrinsic differences in viral replication kinetics and not from a differential effect of the reporters and dyes in viral replication. Together, these results demonstrate the applicability of our

reporter to be used in combination with other molecular sensors, in order to establish a multi-parametric characterization of the infection produced by different flaviviruses.

Discussion

The present study reports the construction of fluorescent protein-based sensors of flavivirus NS2B-NS3 serine proteases activity that become fluorescent upon cleavage by recombinant DENV-2/ZIKV proteases *in vitro* (Fig. 1). Moreover, the variant of this sensor with the internal NS3 cleavage site linker (AAQRRGRIG) reported the highest fluorescence increase in stably-transduced mammalian cells upon DENV-2/ZIKV infection, correlating with the viral induced NS3 protease activity in the cellular context (Fig. 2 and 3). A far-red version of this flavivirus sensor reported the best signal-to-noise ratio in a fluorescent Dulbecco's plaque assay enabling the construction of a multi-reporter platform to study plaque formation with single-cell resolution (Fig. 4 and 5). Finally, the application of this platform revealed important differences in cell-population kinetics of infection and cell death induced by several flaviviruses (Fig. 6).

As a starting point, we developed this genetically encoded flavivirus reporter system by successfully engineering the linker of our previously published caspase-activatable reporters, CA-GFP and CA-mNeptune (26–28), in order to be recognized and cleaved by the flavivirus NS2B-NS3 proteases, giving rise to the FlaviA-GFP and FlaviA-mNeptune reporters, respectively. First, we focused on the validation of three proposed linkers *in vitro* as a proof of concept of the recognition and cleavage of our reporter upon treatment with flavivirus proteases, without the possible effect of other proteases that are present in the cellular context. Our results showed that all three linkers tested were cleaved as soon as one hour post-treatment with both DENV-2 and ZIKV proteases (Fig. 1A and 1B). This fast cleavage validated the amino acid sequences of our linkers as well as the application of “unlinked” versions of both recombinant DENV-2 and ZIKV proteases, in which the NS2B and NS3 regions were produced as independent polypeptides. This choice was based on our own demonstration that the “unlinked”

version of DENV-2 protease rests predominantly in a “closed”, active conformation, in contrast with the less active, relaxed conformation, adopted by the frequently used “linked” construct, in which NS2B and NS3 polypeptides are attached by a nine-amino acid linker (31).

Once the biochemical principle behind the preliminary variants of our reporter was confirmed *in vitro* with recombinant viral proteases, we decided to test its performance upon full flavivirus particles infection in mammalian cells. The highest fluorescence increase to report the infection with DENV-2 and ZIKV in stably transduced BHK-21 cells was obtained with the internal NS3 cleavage site linker (Fig. 2) present in many members of the *Flavivirus* genus (3, 5, 30). Moreover, a BLASTp search of the NCBI reference proteins data base (32) using the query sequence AAQRRGRIG, revealed 100% coverage and 88.9%-100% identity to >60 members of the *Flavivirus* genus. The alignment results included many medically important flaviviruses like WNV, YFV, SEV, DENV, JEV, ZIKV, and TBEV (Fig. S5), among others (1). This finding outlines the potential application of our reporter system to other flaviviruses and supports our hypothesis that the flavivirus internal NS3 cleavage site could represent a conserved viral target for the development of a single antiviral therapy against the members of the *Flavivirus* genus, as previously suggested for DENV (30). Nevertheless, further work using other flaviviruses is needed to establish the whole spectrum of utility and specificity of this reporter system.

Furthermore, our flavivirus reporter system proved to be a useful method for monitoring the kinetics of DENV-2 and ZIKV infection at a single-cell level by live-cell imaging (Fig. 2) and showed a positive correlation with standard virological approaches like detection of viral NS3 protease synthesis and activity by indirect immunofluorescence and western blot (Fig. 3). In this respect, flavivirus reporter replicons have been generated by engineering the viral genomes of reference strains (16–20). However, in recent years special effort has been invested in the development of cell-based molecular reporter systems for live-cell imaging of flavivirus infections (21–23), mainly for their application on the study of native

viral strains and clinical isolates. Among the latter, our system shows some advantages in that it is a fluorescence activatable reporter, which allows an easier interpretation of the results and simplifies the image analysis when compared with those systems based on the relocalization of the fluorescent signal across cellular compartments (21, 23). Moreover, the utility of our fluorescence activation approach arises from its low fluorescent background and the use of a single recombinant construct that codifies for a single fluorescent protein with intramolecular quenching, in contrast with other, difficult to optimize strategies, like the fluorescence resonance energy transfer (FRET) probes (26, 33) and the protease-triggered Cre-mediated reporter system, which rely on the cellular transfection of two different recombinant constructs (22) and could be sensitive to early changes in gene expression. Another great advantage over other systems is that our reporter has been validated with reference strains but also clinical isolates of different flavivirus species like DENV, ZIKV, and YFV, expanding its range of application to more than one flavivirus.

The fluorescence activation principle of our reporter also allowed us to envisage a cell-based fluorescent Dulbecco’s plaque assay for flaviviruses (Fig. 4). The plaque assay is one of the “gold standard” virological techniques originally developed by d’Hérelle for titration and isolation of single clones of bacteriophages and later adapted by Dulbecco to animal viruses (34, 35). Viral plaques arise after genome replication, transcription, translation, virus release from infected cells and infection of surrounding cells (36), thus, plaque development constitutes a hallmark of the infection carried out by a specific viral clone. To date, the kinetics of flavivirus plaque formation could only be monitored for transgenic fluorescent viruses made by modifying the genome of reference strains (16–20). However, we applied the far-red version of our flavivirus sensor to establish, for the first time, a mammalian reporter cell line where the plaque assay can be monitored over time with unlabeled native flavivirus strains. This way, we were able to study the kinetics of viral plaque development with the clinical isolate ZIKV CIET-01 (Fig. 4). Considering that viral plaques are clonal lesions of infected cells formed by the cytopathic effect of replicating viruses (36), we decided to

incorporate molecular sensors for chromatin condensation (Hoechst 33342) and cell death (SYTOX green) to obtain multi-parametric data from single viral plaques. This enabled us to construct a multi-reporter platform to study flavivirus plaque formation with single-cell resolution (Fig. 5), as a way to obtain a preliminary characterization of the infection produced by a particular flavivirus strain.

Following our approach, the quantification of the percentage of cells within each viral plaque corresponding to live-infected, live-infected with chromatin condensation, and dead cells, indicated differential rates of infection and types of induced cell death for DENV-2, ZIKV, and YFV (Fig. 6). The infection with DENV-2 presents the highest proportion of live-infected cells, indicating that the infected cells take longer time to die upon infection and suggesting that this behavior drives to an increased viral production probably related to a faster infection kinetics leading to the formation of larger plaques (37). The amount of DENV-infected cells with chromatin condensation is very similar to that of dead cells, suggesting a fast type of cell demise once the cell death program is engaged, probably necrosis (38, 39). A similar scenario is shown by YFV that induces a fast type of cell death, probably necrosis, but earlier during the infection, which might limit viral spreading leading to a lower proportion of live-infected cells and smaller viral plaques (40). On the other hand, ZIKV has a lower proportion of live-infected cells but a very high number of infected cells with chromatin condensation, suggesting that this viral strain induces a delayed type of cell death, probably apoptosis as previously reported (23, 41–43), preserving for a longer time the cell integrity to produce new viral particles and leading to larger plaques compared to YFV infection (44). However, this could be also related to differences in viral permissiveness of the BHK-21 cell line, since it is known that ZIKV virus tends to infect BHK-21 cells poorly compared to YFV, as demonstrated by envelope protein immunostaining (45, 46). Therefore, our multi-reporter platform serves only as a primary screening of the type of infection exposed by flavivirus strains. A more detailed exploration is needed using virological and cell biology methods to reach strong conclusions about the viral fitness and cell death mechanism induced

by a specific viral strain. Nevertheless, our approach would be suitable for the screening of antiviral compounds by a plaque reduction assay, with the advantage of having a readout of the possible cytotoxicity induced by those compounds in a single experiment.

To our knowledge, this is the first fluorescence activatable cell-based molecular reporter system for live-cell imaging of flavivirus infection, suitable to be used in a plaque assay simultaneously with molecular sensors of other cellular or viral-induced processes. Moreover, taking into account the enormous need for preventative and therapeutic treatments for flavivirus infections like dengue and Zika (47), our multi-reporter platform enables the decoding of viral-specific fingerprints of Dulbecco-plaques formation with a potential future application for antiviral drug research and other studies on viral replication/cell death induction for both native flavivirus strains and clinical isolates.

Experimental procedures

Viruses

Clinical isolate DENV-2 13538 (DENV-2/CR/10066/2007) was provided by Instituto Costarricense de Investigación y Enseñanza en Nutrición y Salud, Cartago, Costa Rica (48). DENV-2 viruses were produced in C6/36 cells from *Aedes albopictus* (ATCC, Manassas, VA) by inoculating a cellular monolayer at a MOI of 0.01 and incubating for 3 days with Roswell Park Memorial Institute medium (RPMI-1640, Gibco, Gaithersburg, MD) supplemented with 2% fetal bovine serum (FBS, Gibco) at 33 °C in an atmosphere of 5% CO₂. Then, culture supernatant was collected, and centrifuged at 3000 x g for 10 min. Before storage at -80 °C, 23% newborn calf serum (NBCS, Gibco) was added (49).

Clinical isolate ZIKV CIET-01 (ZIKV/CR/CIET-01/2016) was kindly provided by Claudio Soto-Garita from Universidad de Costa Rica. Vaccine strain YFV 17D (YFV/US/17D/1937) was isolated from the commercial vaccine YF-VAX® (Sanofi Pasteur, Lyon, France). ZIKV and YFV viruses were produced in Vero cells (ATCC) by inoculating cellular monolayers at a MOI of 0.1 and incubating for 5 days with Minimum Essential Medium

(MEM, Gibco) supplemented with 2% FBS at 37 °C in an atmosphere of 5% CO₂. Culture supernatants were collected, centrifuged at 3000 x g for 10 min and stored at -80 °C.

Viruses were titrated by plaque assay in BHK-21 cells (ATCC) as previously described (50). Briefly, 10-fold serial dilutions of viruses were added to BHK-21 confluent monolayers. After 2 hours of adsorption, cells were incubated at 37 °C in an atmosphere of 5% CO₂ for 5 days with MEM supplemented with 2% FBS and 1% carboxymethylcellulose (Sigma, St. Louis, MO). Plaque numbers were counted after staining with crystal violet. Virus inactivation was carried out by 5 cycles of UV light (254nm) exposure at a energy of 400 000 µJ/cm² in the CL-100 Ultraviolet Crosslinker (UVP, Upland, CA).

Reporter development and molecular cloning

FlaviA-GFP, ZIKVA-GFP, and DENV2A-GFP reporters were developed by site-directed mutagenesis of the linker in the previously described CA-GFP reporter (26–28) to a sequence coding for the flavivirus NS3 internal cleavage site (AAQRRGRIG), the ZIKV polyprotein NS2B/NS3 cleavage site (KTGKRSGAL), and the DENV-2 polyprotein NS2B/NS3 cleavage site (VKKQRAGVL), respectively, using the QuikChange approach (Agilent, Santa Clara, CA). The tRep/control, a truncated variant of the reporter protein, was generated by inserting a stop codon downstream the cleavage site in the linker of the FlaviA-GFP reporter. Then, the genes of the flavivirus-activatable GFP reporters in the plasmid pET21b (Novagen, Madison, WI) were independently amplified by PCR and ligated into the SpeI and XhoI restriction sites of the pLenti-puro vector (a gift from Ie-Ming Shih, Addgene plasmid #39481) (51) to generate the constructs pLenti-ZIKVA-GFP-puro, pLenti-DENV2A-GFP-puro, and pLenti-FlaviA-GFP-puro. Likewise and based on the previously described CA-mNeptune reporter (28), we designed and commercially synthesized (Atum, Newark, CA) the FlaviA-mNeptune reporter gene by changing the linker sequence in order to codify for AAQRRGRIG. Finally, the FlaviA-mNeptune gene in the plasmid pD2109-CMV (Atum) was PCR amplified and ligated into the XbaI and SalI restriction sites of the pLenti-CMV-GFP-Puro vector (a gift from Eric

Campeau, Addgene plasmid #17448) (52) to produce the plasmid pLenti-CMV-FlaviA-mNeptune-puro. All constructs were confirmed by sequencing (Genewiz, South Plainfield, NJ).

Protein expression and purification

FlaviA-GFP, ZIKVA-GFP, DENV2A-GFP, and tRep/control expression constructs in pET21b vectors were transformed into *E. coli* strain BL21(DE3). Flasks containing 2 liters of 2X YT media were inoculated with 8 ml of an overnight culture and grown at 37 °C to an OD₆₀₀ of 0.6. The cultures were then induced using 1 mM Isopropyl β-D-1-thiogalactopyranoside (IPTG, Sigma) and incubated at 20 °C for 5 hours to allow protein expression. Cells were harvested by centrifugation and disrupted by microfluidization. Clarified lysates were prepared by centrifugation at 15,000 x g for 45 min. The reporter proteins were then purified using Co²⁺-affinity liquid chromatography with a 5 ml HiTrap Chelating HP column (GE Healthcare, Chicago, IL). The column was washed with a buffer composed of 50 mM imidazole, 300 mM NaCl, and 50 mM NaH₂PO₄ pH 8.0, and the proteins were eluted using a similar buffer with 300 mM imidazole and stored at 4 °C. Proteins purity was assessed in SDS-PAGE gels stained with Coomassie blue.

DENV-2 protease was expressed as an “unlinked” construct by the co-transformation of BL21(DE3) cells with a pACYDuet plasmid encoding for residues 48-100 of the NS2B cofactor and a pETDuet plasmid comprising amino acids 1-187 of the NS3 protease (a gift from Thomas Keller) (53). ZIKV protease was expressed as an “unlinked” construct by the transformation of BL21(DE3) cells with pET15b vector encoding for amino acids 48-100 of the NS2B cofactor and 1-178 of the NS3 protease (54). The cells harboring either DENV-2 protease or ZIKV protease were grown in 2X YT media with antibiotics at 37 °C to an OD₆₀₀ of 0.6. Protein expression was induced with 1 mM IPTG and proceeded for 3 hours at 25°C. The proteases were purified using Ni²⁺-affinity liquid chromatography with a 5 ml HiTrap Chelating HP column and eluted using a step gradient with 300 mM imidazole. The eluted proteases were further purified using anion exchange with a HiTrap Q HP column (GE Healthcare) with a linear gradient from 10 mM to 500 mM NaCl and stored at -80 °C.

Proteins purity was assessed in SDS-PAGE gels stained with Coomassie blue.

Reporter cleavage and fluorescence assay in vitro

Samples containing 10 μ M of either FlaviA-GFP, ZIKVA-GFP or DENV2A-GFP reporters with and without 10 μ M of DENV-2 or ZIKV proteases were prepared with digestion buffer (50mM Tris buffer pH 8.5, 0,1% CHAPS, 20% glycerol) in a final volume of 120 μ l and added to a costar 96-well black plate. The fluorescence was measured every hour (Ex. 475 nm/Em. 512 nm) for 20 hours at 27 °C. Another set of samples was incubated at 27 °C in 30 μ l aliquots to which SDS loading buffer was added at time points of 0, 1, 5, 10, 15 and 20 hours. These samples were then run on SDS-PAGE and stained with Coomassie blue to determine the cleavage kinetics of the flavivirus-activatable GFP reporters by DENV-2 and ZIKV proteases. Gel images were acquired with a ChemiDoc™ XRS+ System (BioRad, Hercules, CA) and analyzed with the Image J software (NIH, Bethesda, MD) (55) to determine the cleavage efficiency. The fluorescence signal-to-noise ratio was calculated by dividing the signal of the reporter treated with viral protease by the noise gave by the untreated reporter at every time point.

Lentiviral vectors assembly

HEK293T cells (ATCC) were cultured in Dulbecco's modified Eagle medium (DMEM, Gibco) supplemented with 10% FBS, 1X GlutaMAX (Gibco), 1 mM sodium pyruvate (Gibco), and 1X antibiotic-antimycotic solution (Gibco). Lentiviral particles were generated in 60% confluent HEK293T cell monolayers by triple transfection with polyetilenimide (Polysciences, Warrington, PA) of either pLenti-FlaviA-GFP-puro, pLenti-ZIKVA-GFP-puro, pLenti-DENV2A-GFP-puro or pLenti-CMV-FlaviA-mNeptune-puro constructs and both packaging plasmids pMD2.G and psPAX2 (a gift from Didier Trono, Addgene plasmids #12259 and #12260). At 72 hours post-transfection, virus-containing medium was collected, filtered through a 0.45 μ m membrane, supplemented with 5 μ g/mL of polybrene (Sigma), and stored at -80 °C. Finally, 10-fold serial dilutions of each lentiviral seed were added to HEK293T cells and the biological titers in transducing units (TU)/ml were determined by flow cytometry at 48 hours post-transduction using a BD Accuri™ C6

Flow Cytometer (BD Biosciences, Franklin Lakes, NJ), as previously described (56).

Reporter cell lines production and selection

BHK-21 cell monolayers at 80% confluency were stably transduced with lentiviral particles carrying a genetic construct codifying for either FlaviA-GFP, ZIKVA-GFP, DENV2A-GFP or FlaviA-mNeptune reporters. For cell transduction, lentiviral vector particles were added to the cells at a MOI of 1 and centrifuged for 2 hours at 300 x g, 25 °C. At 72 hours post-transduction, cells were selected with 8 μ g/ml of puromycin (Sigma) in MEM 10% FBS during 2 days and then cell populations with homogeneous levels of expression of the constructs were isolated by fluorescence-activated cell sorting with a BD FACSJazz™ Cell Sorter (BD Biosciences) based on the fluorescent basal signal of the reporter proteins. The selected stable cell lines were grown and maintained in MEM supplemented with 10% FBS and 0.5 μ g/ml puromycin.

Infection kinetics in reporter cell lines by live-cell imaging

BHK-21 cells stably expressing the FlaviA-GFP, the ZIKVA-GFP or the DENV2A-GFP reporters were seeded on μ Clear black 96-well plates (Greiner Bio-One, Kremsmünster, Austria) at a density of 15 000 cells per well with MEM supplemented with 2% FBS. After 24 hours of incubation at 37 °C - 5% CO₂, reporter cells were infected with either infectious or UV-inactivated DENV-2 13538 or ZIKV CIET-01 at a MOI of 0.25 and allowed to adsorb for 2 hours at 37°C. After labeling with 1 μ g/mL Hoechst 33342 (Invitrogen, Carlsbad, CA) for 10 minutes, cells were washed with 1X PBS and incubated for 96 hours with FluoroBrite™ DMEM (Gibco) supplemented with 2% FBS and containing 2,5 μ g/mL of propidium iodide (Invitrogen) at 37 °C in an atmosphere of 5% CO₂. Images were acquired every 2 hours with a Cytation 3 Cell Imaging Multi-Mode Reader (BioTek, Winooski, VT). The fluorescence signal-to-noise ratio was calculated by dividing the signal of the reporter cells treated with infectious virus by the noise gave by the reporter cells treated with UV-inactivated virus at every time point.

Kinetic plaque assay on reporter cell lines by live-cell imaging

BHK-21 cells stably expressing the FlaviA-mNeptune reporter were seeded on μ Clear black 96-well plates at a density of 25 000 cells per well with MEM supplemented with 10% FBS. After 24 hours of incubation at 37 °C - 5% CO₂, reporter cells were infected with 10-fold serial dilutions of either infectious or UV-inactivated DENV-2 13538, ZIKV CIET-01, or YFV 17D. After 2 hours adsorption, cells were labeled with 1 μ g/mL Hoechst 33342 for 10 minutes, washed once with 1X PBS and incubated for 120 hours at 37 °C - 5% CO₂ with MEM AutoMod™ (Sigma) supplemented with 2% FBS, 1% carboxymethylcellulose, and 500 nM SYTOX green (Invitrogen). Images of the whole well were acquired every 24 hours with a Cytation 3 Cell Imaging Multi-Mode Reader. Finally, at 120 hours post-inoculation viral plaques were confirmed by crystal violet staining.

Indirect immunofluorescence

At 96 and 120 hours post-infection with either infectious or UV-inactivated DENV-2 13538, medium was removed and cells were fixed for 1 hour with 1% paraformaldehyde (Sigma). Later, cells were permeabilized with 70% ethanol for 15 minutes and 0,001% Triton X-100 (Sigma) for 10 minutes at room temperature. Then, cells were incubated with a 1:800 dilution of rabbit polyclonal anti-DENV NS3 antibody (GeneTex, Irvine, CA, GTX124252) for 1 hour at 37 °C, washed twice with 1X PBS and incubated with a 1:400 dilution of goat polyclonal anti-rabbit IgG Alexa Fluor® 594-conjugated antibody (Invitrogen, A11037) for 30 minutes at 37 °C. After three washes with 1X PBS, FluoroBrite™ DMEM was added and images of the whole well were acquired with a Cytation 3 Cell Imaging Multi-Mode Reader.

Western blot

BHK-21 cells stably expressing the FlaviA-GFP reporter were seeded on 12-well plates (Greiner Bio-One) at a density of 350 000 cells per well with MEM supplemented with 2% FBS. After 24 hours of incubation at 37 °C - 5% CO₂, reporter cells were infected with either infectious or UV-inactivated DENV-2 13538 at a MOI of 0.25 and allowed to adsorb for 2 hours at 37 °C. Every 24 hours during 96 hours of incubation, images were acquired with the Cytation 3 Cell Imaging Multi-

Mode Reader and cells were lysed with 2% SDS solution and stored at -20 °C. Later, samples were run on a SDS-PAGE gel, transferred to a PVDF membrane (Millipore) and blotted in a single step with a mixture of 1:100 dilution of rabbit polyclonal anti-GFP antibody (Invitrogen, A-11122), 1:1000 dilution of rabbit polyclonal anti-DENV NS3 antibody, and 1:500 dilution of rabbit monoclonal anti-vinculin antibody (Invitrogen, 700062). Finally, the membrane was treated with a 1:500 dilution of goat polyclonal anti-rabbit IgG HRP-conjugated antibody (Invitrogen, G-21234) and visualized using the Super Signal West Pico Plus Chemiluminescent Substrate (Thermo Fisher Scientific, Waltham, MA). Images were acquired with a ChemiDoc™ XRS+ System.

Image analysis and statistics

Image analysis was performed with the software CellProfiler 2.0 (<http://www.cellprofiler.org>; Broad Institute, Cambridge, MA). Data are expressed as mean \pm standard deviation (SD) of three independent experiments. Statistical significance of the differences between mean values was determined by using a one-way ANOVA followed by a Tukey's post hoc test with the software SigmaPlot 14 (Systat Software Inc., San Jose, CA). The level of significance is denoted in each figure.

Acknowledgements: We thank Francisco Vega-Aguilar for his technical assistance with viral strains. We thank Joseph P. Kennedy Jr. and Derrick P. Feuerstein for their support and suggestions during the experimentation. We also thank Ralf Bartenschlager, Heidelberg University, for his scientific advice and critical review of the manuscript. This work is dedicated with regard to Alina I. Arias-Barrantes and Alexander Mora-Solano.

Conflict of interest: The authors declare that they have no conflicts of interest with the contents of this article. The content is solely the responsibility of the authors and does not necessarily represent the official views of the National Science Foundation.

Author contributions: J. L. A. and J. A. H. conceptualization; J. L. A. and R. M. methodology; J. L. A., D. J. M., and M. E. H. experimentation; J. L. A. and R. M. data curation and analysis; J. L. A. and R. M. writing-original draft; J. L. A., J. A. H., and R. M. writing-review and editing; J. L. A., J. A. H. and R. M. resources; J. A. H. and R. M. supervision; J. A. H. and R. M. funding acquisition; J. A. H. and R. M. project administration.

References

1. Gould, E., and Solomon, T. (2008) Pathogenic flaviviruses. *Lancet*. **371**, 500–509
2. Lindenbach, B., Murray, C. L., Thiel, H.-J., and Rice, C. M. (2013) Flaviviridae. in *Fields Virology*, pp. 712–746
3. Teo, K. F., and Wright, P. J. (1997) Internal proteolysis of the NS3 protein specified by dengue virus 2. *J. Gen. Virol.* **78**, 337–341
4. Lindenbach, B. D., and Rice, C. M. (2003) Molecular biology of flaviviruses. *Adv. Virus Res.* **59**, 23–61
5. Bera, A. K., Kuhn, R. J., and Smith, J. L. (2007) Functional characterization of cis and trans activity of the flavivirus NS2B-NS3 protease. *J. Biol. Chem.* **282**, 12883–12892
6. Ishikawa, T., Yamanaka, A., and Konishi, E. (2014) A review of successful flavivirus vaccines and the problems with those flaviviruses for which vaccines are not yet available. *Vaccine*. **32**, 1326–1337
7. Scott, L. J. (2016) Tetravalent dengue vaccine: A review in the prevention of dengue disease. *Drugs*. **76**, 1301–1312
8. Normile, D. (2017) Safety concerns derail dengue vaccination program. *Science* (80-.). **358**, 1514–1515
9. Chan, K. W. K., Watanabe, S., Kavishna, R., Alonso, S., and Vasudevan, S. G. (2015) Animal models for studying dengue pathogenesis and therapy. *Antiviral Res.* **123**, 5–14
10. Reynolds, E. S., Hart, C. E., Hermance, M. E., Brining, D. L., and Thangamani, S. (2017) An overview of animal models for arthropod-borne viruses. *Comp. Med.* **67**, 232–241
11. Diamond, M. S., Edgil, D., Roberts, T. G., Lu, B., and Harris, E. (2000) Infection of human cells by dengue virus is modulated by different cell types and viral strains. *J. Virol.* **74**, 7814–23
12. Balsitis, S. J., Coloma, J., Castro, G., Alava, A., Flores, D., Beatty, R., and Harris, E. (2008) Tropism of replicating dengue virus in mice and humans defined by viral nonstructural protein 3-specific immunohistochemistry. *Am. J. Trop. Med. Hyg.* **79**, 38
13. Arias-Arias, J. L., Vega-Aguilar, F., Corrales-Aguilar, E., Hun, L., Loría, G. D., and Mora-Rodríguez, R. (2018) Dengue virus infection of primary human smooth muscle cells. *Am. J. Trop. Med. Hyg.* **99**, 1451–1457
14. Acosta, E. G., and Bartenschlager, R. (2016) The quest for host targets to combat dengue virus infections. *Curr. Opin. Virol.* **20**, 47–54
15. de Wispelaere, M., Lian, W., Potisopon, S., Li, P. C., Jang, J., Ficarro, S. B., Clark, M. J., Zhu, X., Kaplan, J. B., Pitts, J. D., Wales, T. E., Wang, J., Engen, J. R., Marto, J. A., Gray, N. S., and Yang, P. L. (2018) Inhibition of flaviviruses by targeting a conserved pocket on the viral envelope protein. *Cell Chem. Biol.* **25**, 1006–1016
16. Li, S. H., Li, X. F., Zhao, H., Deng, Y. Q., Yu, X. D., Zhu, S. Y., Jiang, T., Ye, Q., Qin, E. De, and Qin, C. F. (2013) Development and characterization of the replicon system of Japanese encephalitis live vaccine virus SA14-14-2. *Virol. J.* **10**, 1–6
17. Schmid, B., Rinas, M., Ruggieri, A., Acosta, E. G., Bartenschlager, M., Reuter, A., Fischl, W., Harder, N., Bergeest, J. P., Flossdorf, M., Rohr, K., Höfer, T., and Bartenschlager, R. (2015) Live

- cell analysis and mathematical modeling identify determinants of attenuation of dengue virus 2'-O-methylation mutant. *PLoS Pathog.* **11**, 1–36
18. Xie, X., Zou, J., Shan, C., Yang, Y., Kum, D. B., Dallmeier, K., Neyts, J., and Shi, P. Y. (2016) Zika virus replicons for drug discovery. *EBioMedicine*. **12**, 156–160
19. Tamura, T., Fukuhara, T., Uchida, T., Ono, C., Mori, H., Sato, A., Fauzyah, Y., Okamoto, T., Kurosu, T., Setoh, Y. X., Imamura, M., Tautz, N., Sakoda, Y., Khromykh, A. A., Chayama, K., and Matsuura, Y. (2017) Characterization of recombinant Flaviviridae viruses possessing a small reporter tag. *J. Virol.* **92**, 1–19
20. Kümmerer, B. M. (2018) Establishment and application of flavivirus replicons. in *Dengue and Zika: Control and antiviral treatment strategies*, pp. 165–173, **1062**, 165–173
21. Medin, C. L., Valois, S., Patkar, C. G., and Rothman, A. L. (2015) A plasmid-based reporter system for live cell imaging of dengue virus infected cells. *J. Virol. Methods*. **211**, 55–62
22. Hsieh, M.-S., Chen, M.-Y., Hsieh, C.-H., Pan, C.-H., Yu, G.-Y., and Chen, H.-W. (2017) Detection and quantification of dengue virus using a novel biosensor system based on dengue NS3 protease activity. *PLoS One*. **12**, 1–19
23. McFadden, M. J., Mitchell-Dick, A., Vazquez, C., Roder, A. E., Labagnara, K. F., McMahon, J. J., Silver, D. L., and Horner, S. M. (2018) A fluorescent cell-based system for imaging zika virus infection in real-time. *Viruses*. **10**, 13–18
24. Winkler, G., Maxwell, S. E., Ruemmler, C., and Stollar, V. (1989) Newly synthesized dengue-2 virus nonstructural protein NS1 is a soluble protein but becomes partially hydrophobic and membrane-associated after dimerization. *Virology*. **171**, 302–305
25. Chung, K. M., Thompson, B. S., Fremont, D. H., and Diamond, M. S. (2007) Antibody Recognition of Cell Surface-Associated NS1 Triggers Fc- Receptor-Mediated Phagocytosis and Clearance of West Nile Virus-Infected Cells. *J. Virol.* **81**, 9551–9555
26. Nicholls, S. B., Chu, J., Abbruzzese, G., Tremblay, K. D., and Hardy, J. A. (2011) Mechanism of a genetically encoded dark-to-bright reporter for caspase activity. *J. Biol. Chem.* **286**, 24977–24986
27. Nicholls, S. B., and Hardy, J. A. (2013) Structural basis of fluorescence quenching in caspase activatable-GFP. *Protein Sci.* **22**, 247–257
28. Wu, P., Nicholls, S. B., and Hardy, J. A. (2013) A Tunable, modular approach to fluorescent protease-activated reporters. *Biophys. J.* **104**, 1605–1614
29. Shiryayev, S. A., Kozlov, I. A., Ratnikov, B. I., Smith, J. W., Lebl, M., and Strongin, A. Y. (2007) Cleavage preference distinguishes the two-component NS2B–NS3 serine proteinases of Dengue and West Nile viruses. *Biochem. J.* **401**, 743–752
30. Constant, D. A., Mateo, R., Nagamine, C. M., and Kirkegaard, K. (2018) Targeting intramolecular proteinase NS2B/3 cleavages for trans -dominant inhibition of dengue virus . *Proc. Natl. Acad. Sci.* **115**, 10136–10141
31. Hill, M. E., Yildiz, M., and Hardy, J. A. (2019) Cysteine disulfide traps reveal distinct conformational ensembles in dengue virus NS2B-NS3 protease. *Biochemistry*. **58**, 776–787
32. Altschul, S. F., Gish, W., Miller, W., Myers, E. W., and Lipman, D. J. (1990) Basic local alignment search tool. *J. Mol. Biol.* **215**, 403–410
33. Leavesley, S. J., and Rich, T. C. (2016) Overcoming limitations of FRET measurements. *Cytom.*

Part A. **89**, 325–327

34. d'Hérelle, F. (1926) The bacteriophage and its behavior. *Nature*. **118**, 183–185
35. Dulbecco, R. (1952) Production of plaques in monolayer tissue cultures by single particles of an animal virus. *Proc. Natl. Acad. Sci.* **38**, 747–752
36. Yakimovich, A., Andriasyan, V., Witte, R., Wang, I. H., Prasad, V., Suomalainen, M., and Greber, U. F. (2015) Plaque2.0-a high-throughput analysis framework to score virus-cell transmission and clonal cell expansion. *PLoS One*. **10**, 1–21
37. Goh, K. C. M., Tang, C. K., Norton, D. C., Gan, E. S., Tan, H. C., Sun, B., Syenina, A., Yousuf, A., Ong, X. M., Kamaraj, U. S., Cheung, Y. B., Gubler, D. J., Davidson, A., St John, A. L., Sessions, O. M., and Ooi, E. E. (2016) Molecular determinants of plaque size as an indicator of dengue virus attenuation. *Sci. Rep.* **6**, 1–11
38. Ghosh Roy, S., Sadigh, B., Datan, E., Lockshin, R. A., and Zakeri, Z. (2014) Regulation of cell survival and death during Flavivirus infections. *World J. Biol. Chem.* **5**, 93–105
39. Galluzzi, L., Vitale, I., Aaronson, S. A., Abrams, J. M., Adam, D., Agostinis, P., Alnemri, E. S., Altucci, L., Amelio, I., and Andrews, D. W. et al. (2018) Molecular mechanisms of cell death: Recommendations of the Nomenclature Committee on Cell Death 2018. *Cell Death Differ.* **25**, 486–541
40. Liprandi, F. (1981) Isolation of plaque variants differing in virulence from the 17D strain of yellow fever virus. *J. Gen. Virol.* **56**, 363–370
41. Liu, J., Li, Q., Li, X., Qiu, Z., Li, A., Liang, W., Chen, H., Cai, X., Chen, X., Duan, X., Li, J., Wu, W., Xu, M., Mao, Y., Chen, H., Li, J., Gu, W., and Li, H. (2018) Zika virus envelope protein induces G2/M cell cycle arrest and apoptosis via an intrinsic cell death signaling pathway in neuroendocrine PC12 cells. *Int. J. Biol. Sci.* **14**, 1099–1108
42. Limonta, D., Jovel, J., Kumar, A., Airo, A. M., Hou, S., Saito, L., Branton, W., Wong, G. K. S., Mason, A., Power, C., and Hobman, T. C. (2018) Human fetal astrocytes infected with zika virus exhibit delayed apoptosis and resistance to interferon: Implications for persistence. *Viruses*. **10**, 1–19
43. Anfasa, F., Goeijenbier, M., Widagdo, W., Siegers, J. Y., Mumtaz, N., Okba, N., van Riel, D., Rockx, B., Koopmans, M. P. G., Meijers, J. C. M., and Martina, B. E. E. (2019) Zika Virus Infection Induces Elevation of Tissue Factor Production and Apoptosis on Human Umbilical Vein Endothelial Cells. *Front. Microbiol.* **10**, 1–11
44. Kato, F., Tajima, S., Nakayama, E., Kawai, Y., Taniguchi, S., Shibasaki, K., Taira, M., Maeki, T., Lim, C. K., Takasaki, T., and Saijo, M. (2017) Characterization of large and small-plaque variants in the Zika virus clinical isolate. *Sci. Rep.* **7**, 1–3
45. Chan, J. F. W., Yip, C. C. Y., Tsang, J. O. L., Tee, K. M., Cai, J. P., Chik, K. K. H., Zhu, Z., Chan, C. C. S., Choi, G. K. Y., Sridhar, S., Zhang, A. J., Lu, G., Chiu, K., Lo, A. C. Y., Tsao, S. W., Kok, K. H., Jin, D. Y., Chan, K. H., and Yuen, K. Y. (2016) Differential cell line susceptibility to the emerging Zika virus: implications for disease pathogenesis, non-vector-borne human transmission and animal reservoirs. *Emerg. Microbes Infect.* **5**, e93
46. Petrova, E., Gracias, S., Beauclair, G., Tangy, F., and Jouvenet, N. (2019) Uncovering flavivirus host dependency factors through a genome-wide gain-of-function screen. *Viruses*. **11**, 1–17
47. Zakaria, M. K., Carletti, T., and Marcello, A. (2018) Cellular targets for the treatment of flavivirus

- p. 15D.2.1-15D.2.24
-
- infections.
- Front. Cell. Infect. Microbiol.*
- 8**
- , 1–11
-
48. Soto-Garita, C., Somogyi, T., Vicente-Santos, A., and Corrales-Aguilar, E. (2016) Molecular characterization of two major dengue outbreaks in Costa Rica.
- Am. J. Trop. Med. Hyg.*
- 95**
- , 201–205
-
49. Medina, F., Medina, J. F., Colon, C., Vergne, E., Santiago, G. A., and Munoz-Jordan, J. L. (2012) Dengue virus: Isolation, propagation, quantification, and storage. in
- Current Protocols in Microbiology*
- , p. 15D.2.1-15D.2.24
-
50. Morens, D. M., Halstead, S. B., Repik, P. M., Putvatana, R., and Raybourne, N. (1985) Simplified plaque reduction neutralization assay for dengue viruses by semimicro methods in BHK-21 cells: comparison of the BHK suspension test with standard plaque reduction neutralization.
- J. Clin. Microbiol.*
- 22**
- , 250–4
-
51. Guan, B., Wang, T. L., and Shih, I. M. (2011) ARID1A, a factor that promotes formation of SWI/SNF-mediated chromatin remodeling, is a tumor suppressor in gynecologic cancers.
- Cancer Res.*
- 71**
- , 6718–6727
-
52. Campeau, E., Ruhl, V. E., Rodier, F., Smith, C. L., Rahmberg, B. L., Fuss, J. O., Campisi, J., Yaswen, P., Cooper, P. K., and Kaufman, P. D. (2009) A versatile viral system for expression and depletion of proteins in mammalian cells.
- PLoS One.*
- 4**
- , e6529
-
53. Kim, Y. M., Gayen, S., Kang, C. B., Joy, J., Huang, Q., Chen, A. S., Wee, J. L. K., Ang, M. J. Y., Lim, H. A., Hung, A. W., Li, R., Noble, C. G., Lee, L. T., Yip, A., Wang, Q. Y., Chia, C. S. B., Hill, J., Shi, P. Y., and Keller, T. H. (2013) NMR analysis of a novel enzymatically active unlinked dengue NS2B-NS3 protease complex.
- J. Biol. Chem.*
- 288**
- , 12891–12900
-
54. Hill, M. E., Kumar, A., Wells, J. A., Hobman, T. C., Julien, O., and Hardy, J. A. (2018) The unique cofactor region of Zika virus NS2B-NS3 protease facilitates cleavage of key host proteins.
- ACS Chem. Biol.*
- 13**
- , 2398–2405
-
55. Schneider, C. A., Rasband, W. S., and Eliceiri, K. W. (2012) NIH Image to ImageJ: 25 years of image analysis.
- Nat. Methods.*
- 9**
- , 671–675
-
56. Tiscornia, G., Singer, O., and Verma, I. M. (2006) Production and purification of lentiviral vectors.
- Nat. Protoc.*
- 1**
- , 241–245

FOOTNOTES

This work was supported by Universidad de Costa Rica (project VI-803-B9-505), National Science Foundation (Grant NSF CBET1511367, to J. A. H.), and International Centre for Genetic Engineering and Biotechnology (Grant CRP/19/004, to R. M.).

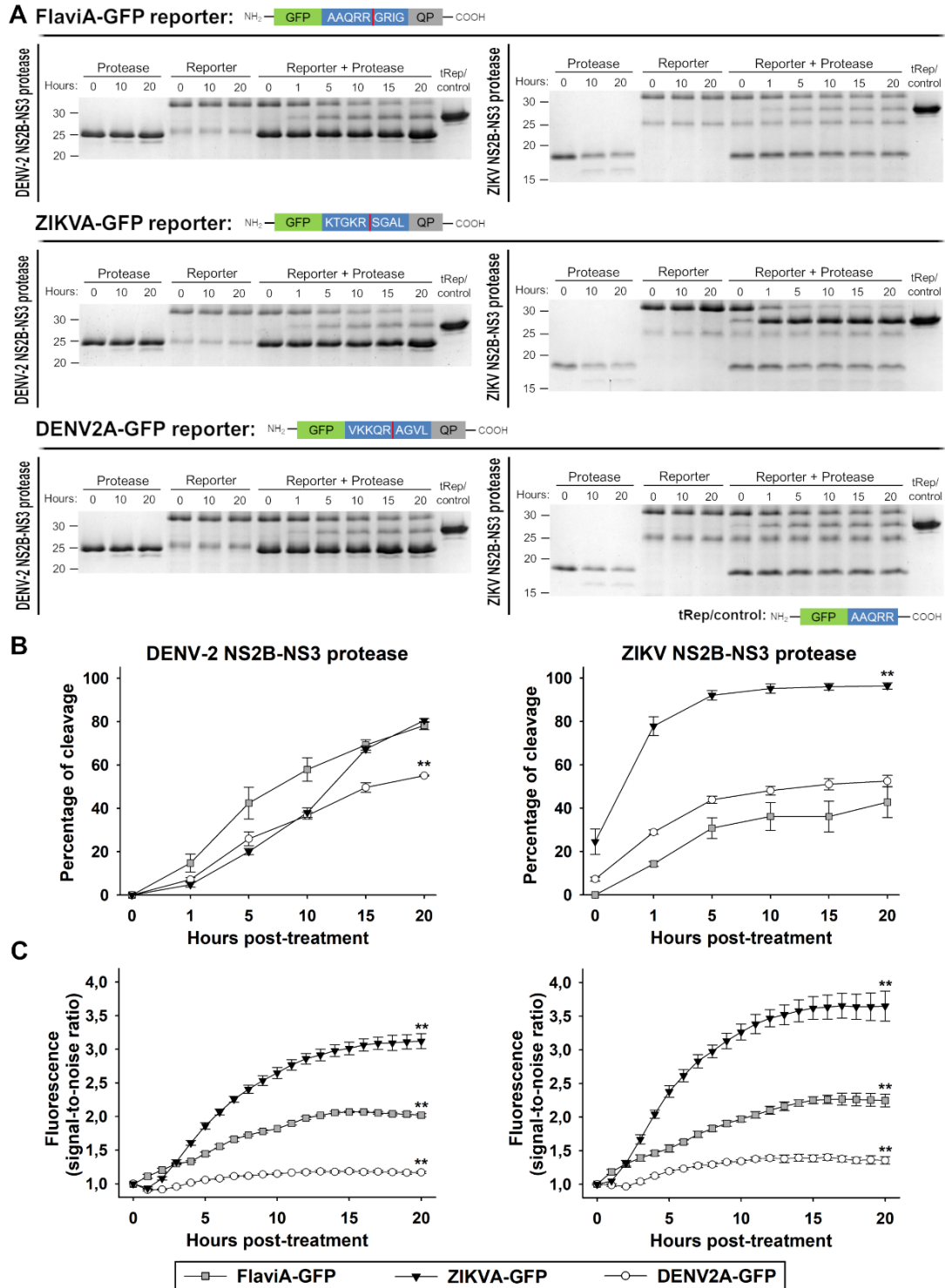


Figure 1. Fluorescence activatable GFP-based reporters for flavivirus NS2B-NS3 protease activity become fluorescent upon cleavage by DENV-2/ZIKV recombinant proteases *in vitro*. The flavivirus-activatable GFP reporters contain a quenching peptide (QP) at the C-terminus of GFP joined by a linker consisting of a cleavage site for the flavivirus NS2B-NS3 proteases. When the viral proteases cleave the linker, the quenching peptide is removed and the GFP adopts a conformation promoting chromophore maturation. Three variants of this reporter were developed by changing the linker sequence: ZIKVA-GFP

(ZIKV polyprotein NS2B/NS3 cleavage site linker), DENV2A-GFP (DENV-2 polyprotein NS2B/NS3 cleavage site linker), and FlaviA-GFP with the internal NS3 cleavage site linker which is present in many members of the *Flavivirus* genus. **(A)** *In vitro* cleavage kinetics of the flavivirus-activatable GFP reporter. Purified reporter proteins were mixed with purified DENV-2 NS2B-NS3 protease (left panel) or ZIKV NS2B-NS3 protease (right panel) at a molar ratio of 1:1 and incubated for given times. Reactions were quenched by thermal treatment in SDS loading buffer and samples were analyzed by SDS-PAGE and staining of the gels with Coomassie blue. tRep/control is an engineered cleaved variant of the FlaviA-GFP protein and was used as size marker of cleaved reporters. Representative cropped images from three independent experiments are shown. **(B)** Cleavage efficiency kinetics of the purified flavivirus-activatable GFP reporter proteins treated with purified DENV-2 NS2B-NS3 protease (left) and ZIKV NS2B-NS3 protease (right). **(C)** Time-resolved fluorescence signal-to-noise ratio of the purified flavivirus-activatable GFP reporter proteins treated with purified DENV-2 NS2B-NS3 protease (left) and ZIKV NS2B-NS3 protease (right). Data are expressed as mean \pm SD of three independent experiments. $**p < 0.001$ compared to the other two reporter variants at 20 hours post-treatment.

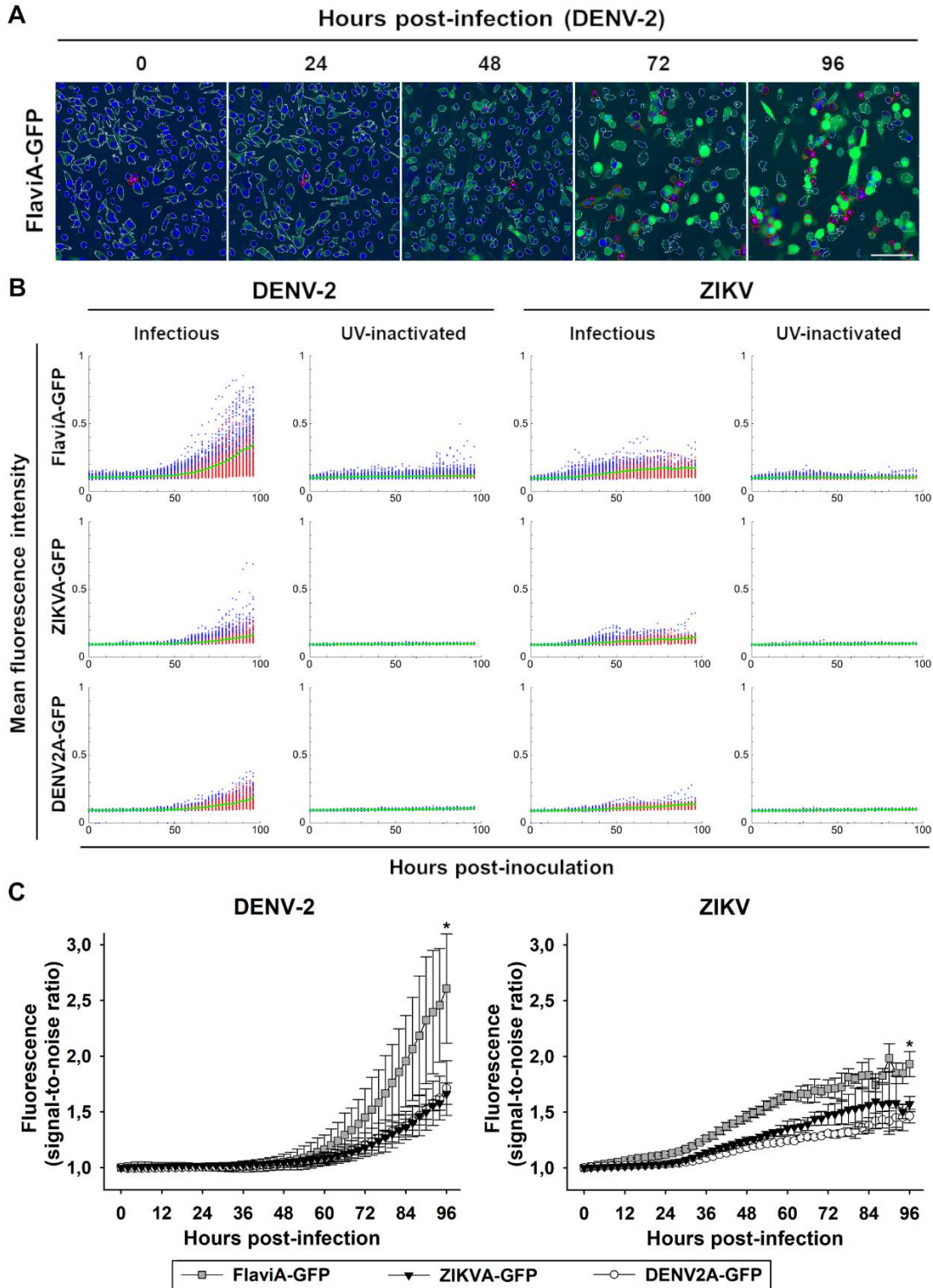


Figure 2. The FlaviA-GFP sensor reports the highest fluorescence increase in stably-transduced mammalian cells upon DENV-2/ZIKV infection. We generated three BHK-21 stable cell lines expressing the flavivirus-activatable GFP reporters, each with one of the previously tested linker sequences. After cell sorting of subpopulations with homogeneous expression of each reporter, cells were grown and infected with either infectious or UV-inactivated DENV-2 13538/ZIKV CIET-01 at a low MOI of 0.25, for the specified time periods. (A) An automated image analysis protocol was constructed in CellProfiler 2.0 for

the quantification of live (white outline), dead (red outline) and activated FlaviA-GFP fluorescent cells (green). A representative experiment is shown for the FlaviA-GFP stable cell line infected with DENV-2 (n = three independent experiments, magnification of 200X, scale bar = 100 μ m). **(B)** The flavivirus-activatable GFP reporters activation is represented by scatter plots showing the time-resolved fluorescence of the population of single live (blue) and dead (red) reporter cells after the exposure to infectious or UV-inactivated DENV-2 (left) or ZIKV (right). The population mean values for each condition are represented by the green continuous lines. Representative scatter plots are shown (n = three independent experiments). **(C)** The cell population kinetics of the flavivirus-activatable GFP sensors fluorescence across multiple experiments confirmed that the flavivirus internal NS3 cleavage site linker (AAQRRGRIG) confers the highest signal-to-noise ratio to report the infection with both DENV-2 (left) and ZIKV (right) in stably transduced BHK-21 cells. Data are expressed as mean \pm SD of three independent experiments. * $p < 0.05$ compared to both ZIKVA-GFP and DENV2A-GFP at 96 hours post-infection.

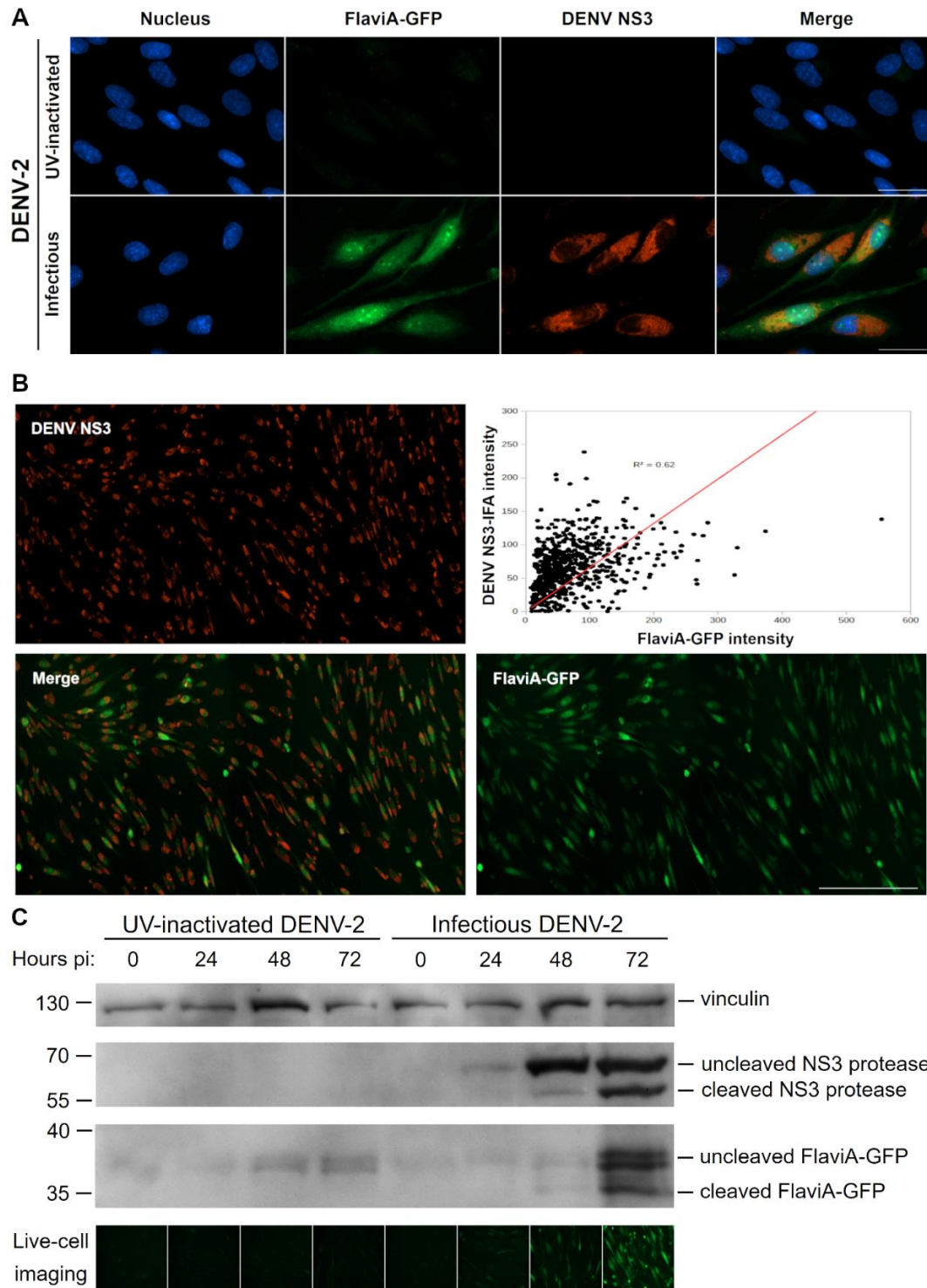


Figure 3. The FlaviA-GFP reporter becomes cleaved and fluorescent in stably-transduced BHK-21 cells upon DENV-2 infection, which correlates with the viral NS3 protease synthesis and autoproteolysis. Stable BHK-21 cells expressing the FlaviA-GFP reporter were infected with either infectious or UV-inactivated DENV-2 13538 at a low MOI of 0.25, for the specified time periods post-inoculation (pi). (A) Comparison of DENV-2 infection detection by the FlaviA-GFP reporter (green) and immunostaining with an anti-DENV NS3 protease antibody (orange) in stably-transduced BHK-21 cells at

72 hours post-infection with DENV-2. Images from a representative experiment are shown (n = three independent experiments, magnification of 600X, scale bar = 30 μ m). **(B)** Correlation of the total cell fluorescence intensity given by the FlaviA-GFP reporter (green) and an immunofluorescence assay (IFA) with an anti-DENV NS3 protease antibody (orange) in stably transduced BHK-21 cells at 72 hours post-infection with DENV-2. A representative experiment is shown (n = three independent experiments, magnification of 200X, scale bar = 300 μ m). **(C)** Cleavage and fluorescence kinetics of the FlaviA-GFP reporter in stable BHK-21 cells upon DENV-2 infection and subsequent viral NS3 protease production and activity. A representative western blot kinetics with its corresponding live-cell images set is shown (n = three independent experiments, magnification of 200X, scale bar = 100 μ m).

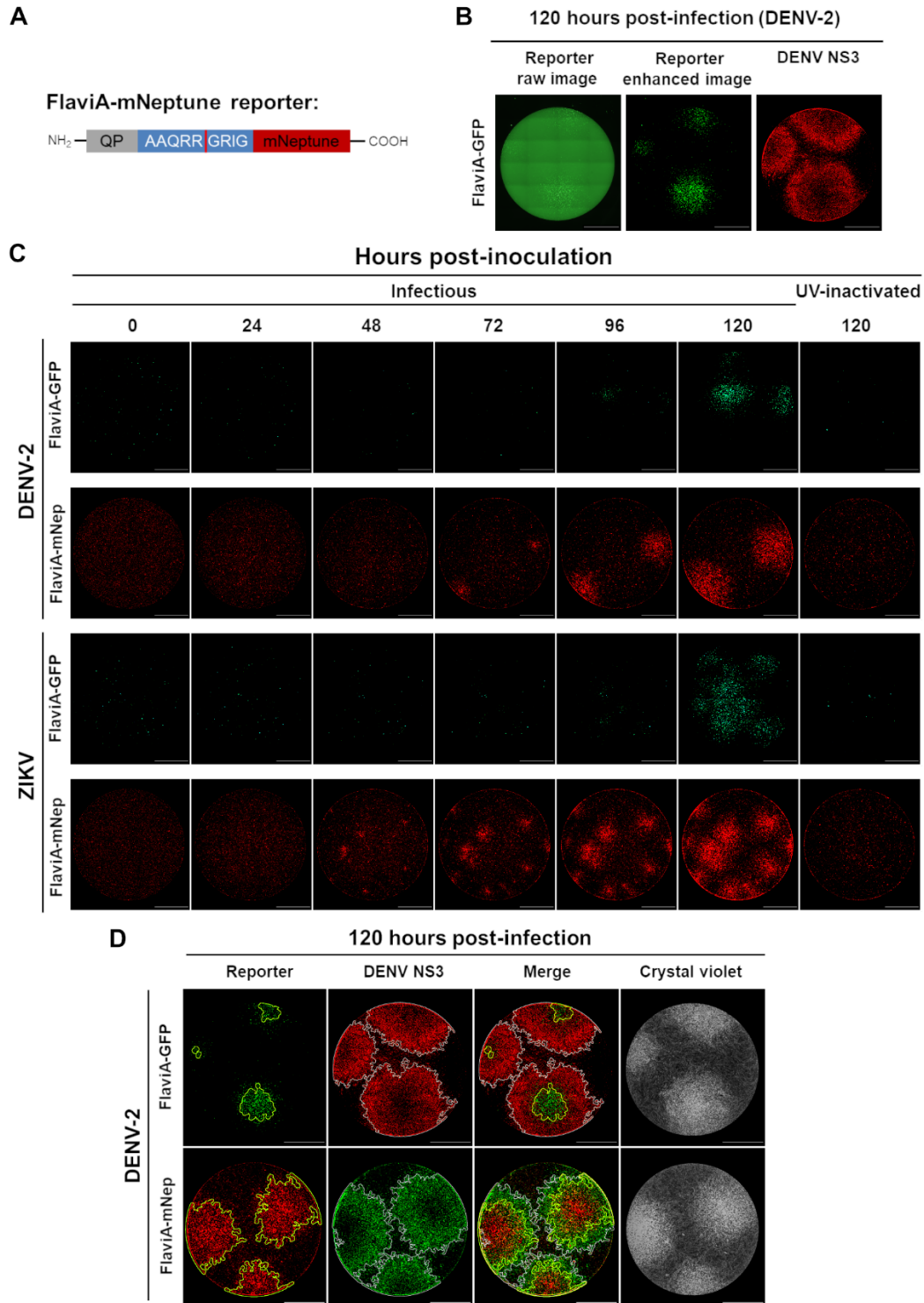


Figure 4. The FlaviA-mNeptune is a far-red version of the flavivirus reporter that enables earlier detection of the cell infection kinetics in a DENV-2/ZIKV plaque assay. We generated two BHK-21 stable cell lines expressing either a green or a far-red version of the flavivirus reporter. Both versions were compared by plaque assay upon infection with DENV-2 13538 and ZIKV CIET-01 at the specified time periods. (A) The FlaviA-mNeptune reporter is a quenched version of the fluorescent protein mNeptune which contains a quenching peptide (QP) at the N-terminus joint by a linker consisting of the internal NS3

cleavage site (AAQRRGRIG), which is conserved among many members of the *Flavivirus* genus. When the flavivirus protease cleaves the linker the quenching peptide is removed and the mNeptune adopts its fluorescent structural conformation. **(B)** BHK-21 cells stably-transduced with the FlaviA-GFP reporter and infected with DENV-2 required a contrast enhancement procedure to reveal viral plaques at 120 hours post-infection but with a poor correlation when compared with the same plaques labeled with an anti-DENV NS3 protease antibody. **(C)** The plaque assay kinetics showed that BHK-21 cells stably-transduced with the FlaviA-mNeptune reporter accumulate enough intensity to reveal fluorescent plaques by 48 and 72 hours post-infection with ZIKV and DENV-2, respectively, much earlier than their counterparts transduced with the FlaviA-GFP reporter. **(D)** The performance of both GFP and mNeptune reporters was further evaluated by comparing the size of their resulting fluorescent plaques to the signal reported by an anti-DENV NS3 protease antibody and crystal violet staining, confirming that the FlaviA-mNeptune reporter has a better correlation to both the infection front (DENV NS3 immunostaining) and the cytopathic effect (crystal violet staining), compared to the FlaviA-GFP reporter. A representative experiment for each condition is shown (n = three independent experiments, magnification of 40X, scale bar = 1000 μ m).

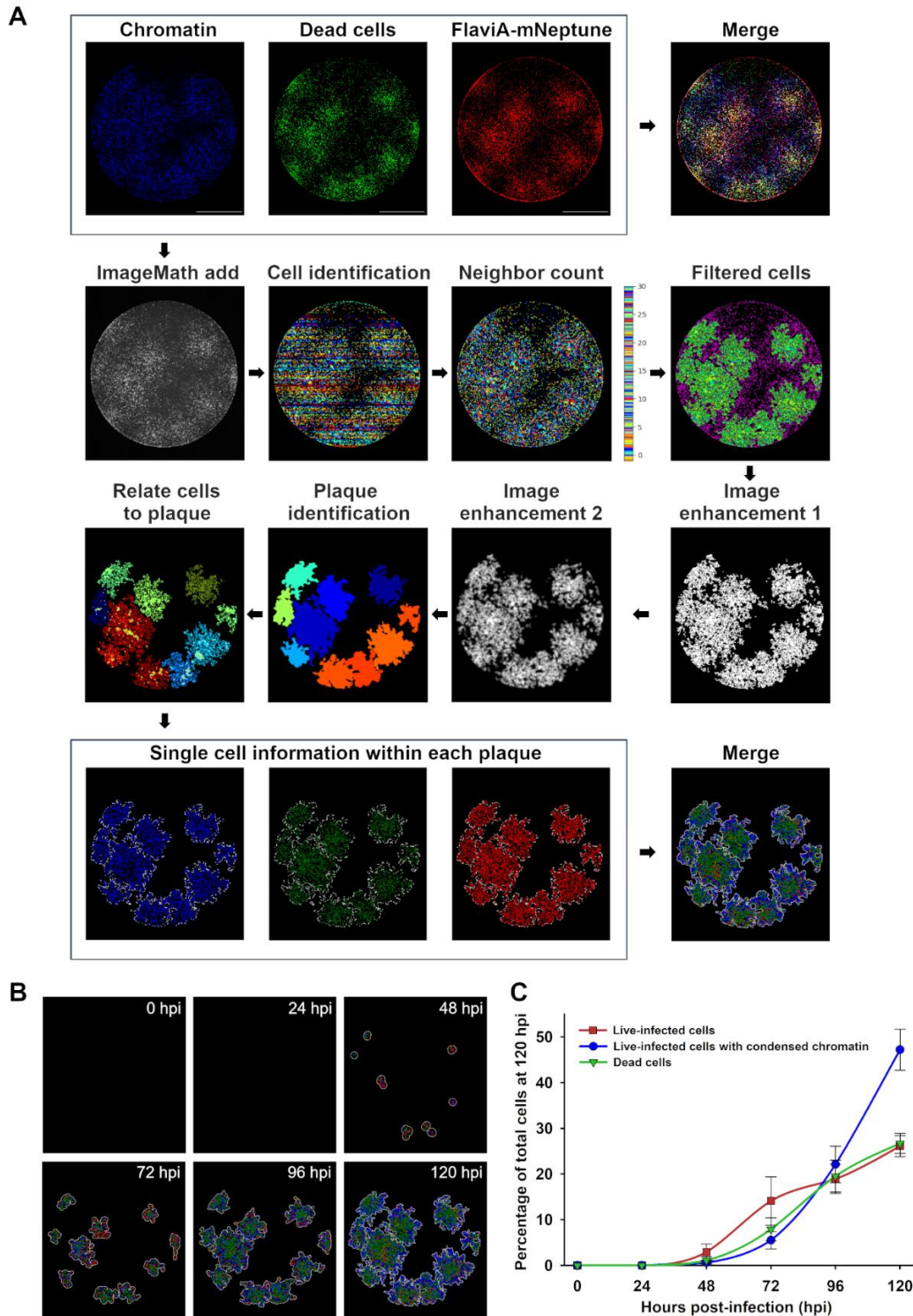


Figure 5. The FlaviA-mNeptune reporter enables analysis of the kinetics of ZIKV infection and induced cell death in single-plaques and single-cells. We constructed an image analysis protocol using the software CellProfiler 2.0 to characterize the kinetics of infection and cell death by the quantification of fluorescence features of cells imaged to assess DNA/chromatin condensation (Hoechst 33342), cell death (SYTOX green), and viral infection (FlaviA-mNeptune reporter). **(A)** High resolution images were stitched into a single image of the well for all three fluorescent channels, which intensities were added into a single

image to have a redundant single-cell identification. A neighbor count and threshold were performed in order to filter the cells belonging to plaques and achieve single plaque identification. The single cells previously identified were related to their respective parent plaques in order to quantify single-cell parameters within each plaque, including chromatin condensation (blue), cell death (green), and the intensity of the FlaviA-mNeptune reporter (red). **(B)** The image analysis protocol was applied to analyze a representative kinetics of ZIKV plaque formation during 120 hours post-infection (hpi), achieving the identification of individual plaques and the categorization of single cells within each plaque as live-infected (red), live-infected with chromatin condensation (blue), and dead (green). The 120 hpi image was reused from point A, as its generation was used in Fig. 5A to exemplify the image analysis pipeline applied to analyze the viral plaques at every post-infection time depicted in Fig. 5B. **(C)** Time-resolved kinetics of ZIKV infection described by parameters of percentage of live-infected cells (red), live-infected cells with chromatin condensation (blue), and dead cells (green) within the viral plaques. Images and data from a representative analyzed experiment are shown (n = three independent experiments, magnification of 40X, scale bar = 1000 μ m). Data are expressed as mean \pm SD for the number of plaques identified at each time point depicted.

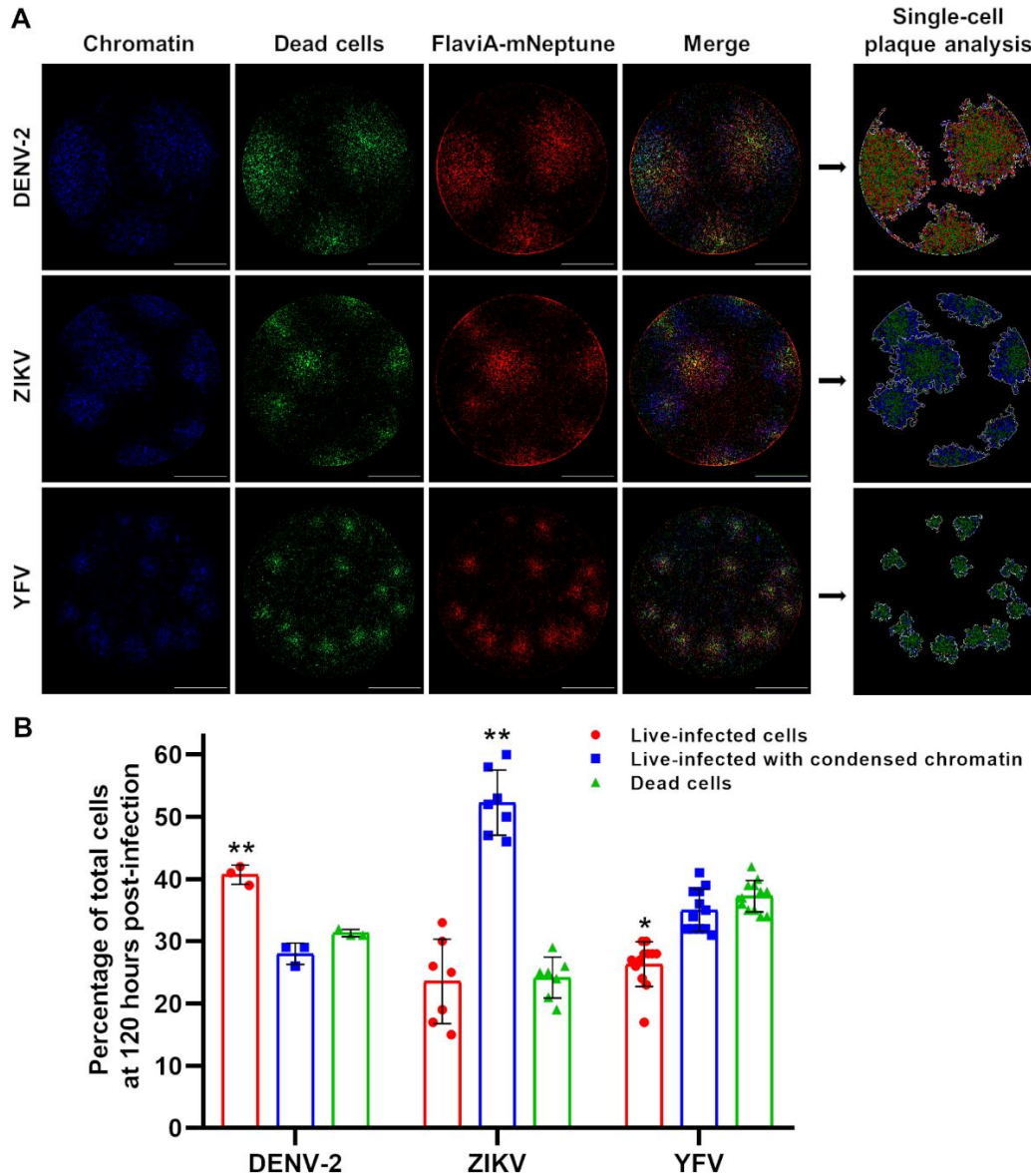


Figure 6. The FlaviA-mNeptune reporter enables the comparative characterization of the infection produced by flaviviruses in terms of viral replication and induced cell death at a single-cell level. We applied our image analysis protocol to characterize the DENV, ZIKV, and YFV infection and induced cell death by the quantification of fluorescence features of cells imaged to assess DNA/chromatin condensation (Hoechst 33342), cell death (SYTOX green), and viral infection (FlaviA-mNeptune reporter). **(A)** The image analysis protocol was applied to achieve the identification of viral plaques produced by DENV, ZIKV, and YFV at 120 hours post-infection (hpi) and the categorization of single cells within each plaque as live-infected (red), live-infected with chromatin condensation (blue), and dead (green). **(B)** DENV, ZIKV, and YFV infection described by parameters of percentage of live-infected cells (red), live-infected cells with chromatin condensation (blue), and dead cells (green) within the viral plaques at 120 hpi. Images and data from a representative analyzed experiment are shown ($n =$ three independent experiments, magnification of 40X, scale bar = 1000 μ m). Data are expressed as mean \pm SD for the number of plaques generated by each virus. * $p < 0.05$, ** $p < 0.001$ compared to the other two cell populations conforming the plaques of the same viral species.

**A fluorescence activatable reporter of flavivirus NS2B-NS3 protease activity enables
live imaging of infection in single cells and viral plaques**

Jorge L. Arias-Arias, Derek J. MacPherson, Maureen E. Hill, Jeanne A. Hardy and Rodrigo
Mora-Rodríguez

J. Biol. Chem. published online January 9, 2020

Access the most updated version of this article at doi: [10.1074/jbc.RA119.011319](https://doi.org/10.1074/jbc.RA119.011319)

Alerts:

- [When this article is cited](#)
- [When a correction for this article is posted](#)

[Click here](#) to choose from all of JBC's e-mail alerts